2013

Discrete time modeling and control of DC/DC switching converter for solar energy systems

Shaghayegh Kazemlou
Louisiana State University and Agricultural and Mechanical College

DISCRETE TIME MODELING AND CONTROL OF DC/DC SWITCHING CONVERTER FOR SOLAR ENERGY SYSTEMS

A Thesis

Submitted to the Graduate Faculty of the
Louisiana State University and
Agricultural and Mechanical College
in partial fulfillment of the
requirements for the degree of
Master of Science in Electrical Engineering

in

Department of Electrical and Computer Engineering

by
Shaghayegh Kazemlou
B.S., Sharif University of Technology, 2007
M.S., Sharif University of Technology, 2010
December 2013

ACKNOWLEDGEMENTS

I would like to express my appreciation to my major professor Dr. Shahab Mehraeen, for his encouragement and invaluable guidance throughout the research.

I would also like to acknowledge the invaluable help and assistance from Dr. Ernest Mendrela, Dr. Leszek S. Czarnecki and Mr. Michael McAnelly as members of the committee.

I would also like to thank all my friends, colleagues and everyone from Louisiana State University who helped me throughout my dissertation research.

TABLE OF CONTENTS

ABSTRACT

Distributed generation networks including micro grids benefit from solar cells that are controlled by dc-dc converters. In this research a nonlinear discrete-time model for a buck converter tied to a solar system is derived with unknown internal dynamics. Then, adaptive neural network (NN) controller is employed to enhance stability of dc-dc converter connected to grid-tie inverter (GTI) in the presence of power system disturbances. The NN weights are tuned online by using a novel update law. By using Lyapunov techniques, all signals can be shown to be uniformly ultimately bounded (UUB). In addition, the interaction of the converter with the GTI is investigated to assure stability of the entire interconnected system while the GTI is controlled via a novel stabilizer similar to power system stabilizer (PSS). The proposed nonlinear discrete-time converter controller along with the GTI, equipped with PSS, is simulated in Matlab Simulink environment. The results have highlighted the effectiveness of the proposed modeling and controller design.

CHAPTER 1
INTRODUCTION

1.1 Introduction

Increasing electricity demands, environmental pollution due to the widespread utilization of fossil fuels and the limited resources of oil and gas are among the serious concerns in recent years. Therefore, renewable distributed generation including solar, hydro, biogas, biomass and wind, has attracted significant attention since it offers a potential solution to these problems. Among the renewable resources, the photovoltaic (PV) power generation systems are becoming ubiquitous due to their simple and noiseless operation as well as availability of solar power. However, the output electric characteristics of the solar cells are highly nonlinear rendering its power very sensitive to the output voltage [1],[2]. For maximum utilization efficiency, it is necessary to match the PV generator output voltage to that of the load such that the operating points of the PV generator and load coincide (preferably at the maximum power point (MPP) of PV.) In order to adjust the operating point of the PV generator, a dc-dc converter is incorporated to the system as an interface between the solar array and the GTI connecting the solar array to the power network. As the PV generator and the GTI interact with each other, due to their inherent non-linearity and lack of inertia, the system is potentially subject to oscillations resulting from network disturbances [3], etc. These properties have been taken into account in this research through modeling and control of the dc-dc converter and GTI.

1.2 Research Objective

The power system comprised of synchronous and renewable generators is considered in this research where GTIs are used to interface the renewable energy sources to the grid in order to control the delivered power.

In this work a nonlinear discrete-time model for a solar-system-connected buck converter is developed. The control input is the duty cycle, which is a discrete-time variable and is altered at the beginning of each switching period. Next, adaptive NN controller is utilized to obtain a stable dc-dc converter.

Next, the renewable generator (RG) is modeled to behave as a synchronous generator (SG) with similar dynamics where the dc-link capacitor acts as the energy storage similar to the rotor of a SG. The GTI is equipped with an observer/controller that models the GTI similar to a synchronous generator, and thus, makes available the utilization of excitation-like damping controller that aims at stabilizing the inverter dc-link capacitor. Here, the proposed inverter observer/controller is an improved version of a mechanism proposed by the authors in their past work [4] that is able to employ a control signal from excitation-like mechanisms in order to stabilize the GTI dc-link capacitor voltage.

Besides, the dc-dc converter is separately controlled by the proposed adaptive NN discrete-time controller and decoupled from the GTI in this work. The NN controller employs a novel update law that prevents the NN weight estimates from remaining large after the regulation error becomes small, as opposed to conventional update laws [5],[6]. The performance of the nonlinear discrete-time dc-dc converter controller is evaluated in simulation carried out in Matlab/Simulink environment. The corresponding results have highlighted the effectiveness of the proposed modeling and controller design in stabilizing PV generator output power as well as the stability of the inverter dc-link voltage in the presence of the power system disturbances.

1.3 Background and Literature Review

Stability, protection, and operational restrictions in integration of distributed energy sources, have been investigated extensively in the literature in both dc-dc and dc-ac parts using

different levels of simplifications and assumptions for modeling the components of the system [7]-[20]. Most of these research works have assumed linear models and infinite-bus connection [3]. The maximum power voltage (MPV)-based approaches have been developed in [2], [7], and [8] but the dynamics of the dc-dc converter are not taken into account. The works of [9]-[13] propose a dynamic model of solar dc-dc converter neglecting the converter input voltage dynamics, which can affect the solar output power. In [14] a dynamical model for a buck converter is described by the state equations and power system stability analysis has been introduced using a linearized system model in the presence of the renewable energy sources. However, this method implies that the states variations are in a small region around the operating point. For a more accurate description the dc-dc converter is modeled in discrete-time [20],[21]. However, interaction of the inherently nonlinear solar cells with the dc-dc converter is not investigated.

On the other hand, stability issues of power systems involving GTI controlled by droop controllers has been the subject of several studies [15],[16] in which small-signal state-space modeling and analysis of a micro grid are presented. In [16] the model was analyzed in terms of the system eigenvalues and their sensitivity to different states where it is shown that the dominant eigenvalues are caused by the droop controller. In [17]-[19] various dynamical models of renewable energy sources and the interfacing power electronics are introduced. However, it is always assumed that the renewable source is connected to an infinite bus, an assumption that is not valid if the share of renewable energy sources is significant or the power system does not have large amounts of stored energy. In this research a nonlinear discrete-time model for a buck converter tied to a solar system is derived with unknown internal dynamics. Then, adaptive

neural network (NN) controller is employed to enhance stability of dc-dc converter connected to grid-tie inverter (GTI) in the presence of power system disturbances.

CHAPTER 2
GRID-CONNECTED RENEWABLE SYSTEM

2.1 Introduction

In this chapter the solar power generation system is elaborated, which is comprised of solar panels, a dc-dc buck converter, and a GTI interfacing the ac network.

2.2 Solar System Model

Solar power generation system comprised of solar panels, a dc-dc buck converter and a GTI is depicted in Figure 1.

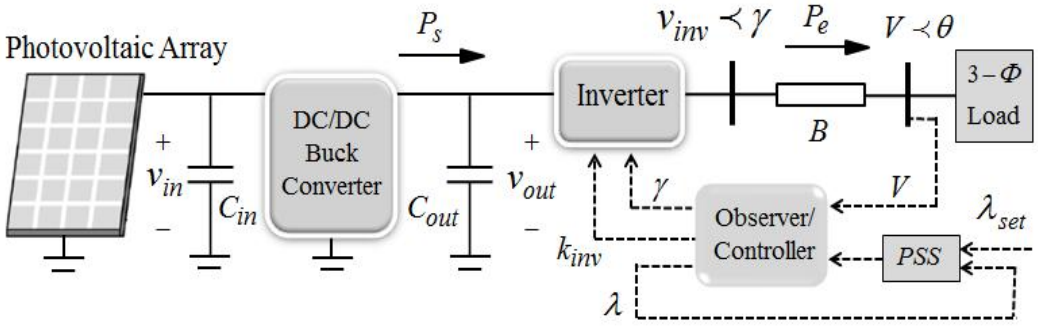

Figure 1 Solar power generation system

When a disturbance occurs in the power network the capacitors' energies deviate from their normal operating values due to the imbalance caused by the perturbation. If there is no controller to mitigate the oscillations, the power system will face power oscillations and a potential instability which prevents the system from returning to its normal operating states. The disturbance affects the converter and GTI states as well as power network voltages and angles. In order to diminish the oscillations and improve the system dynamics, the power electronics interfaces consisting the dc-dc converter and the GTI need to be controlled through proper modeling and control designs. In [4], the GTI is modeled as a synchronous generator with an excitation-like control input. Thus, conventional synchronous generator control methods are applicable to the GTI connecting renewable generator to the grid.

2.3 Grid-Tie Inverter

A large number of renewable energy systems (especially in distributed generation power systems and micro grids) are connected to the main grid through a GTI that is shown in Figure 1.

As opposed to some conventional methods that assume an infinite bus when renewable sources are considered [17]-[19], here a differential-algebraic model of the ac and dc components of a GTI is presented in which the angle of inverter's output voltage, the capacitor's stored energy and the associated controller dynamics will have equivalent dynamical behaviors as those of a synchronous generator. Thus, all known control strategies for a multi-machine power system with excitation control such as AVR (automatic voltage regulator), PSS and nonlinear controllers can be utilized to control the renewable energy sources. This chapter is continued by a brief introduction to synchronous generator equations and the GTI modeling and control. The detailed modeling and control characteristics for the dc-dc part are stated in the next chapter.

In the two-axis model [4], synchronous generator dynamical equations are given as

$$
\begin{aligned}
\dot{¢} &= \mu \\
\dot{\mu} &= \frac{1}{M}\left(P_m - P_e\right) \\
\dot{E}'_q &= \frac{1}{T_{d0}}\left(-\frac{x_d}{x'_d}E'_q + \frac{x_d - x'_d}{x'_d}V\cos(¢ - \bar{}) + E_{fd}\right) \\
\dot{E}'_d &= \frac{1}{T_{q0}}\left(-\frac{x_q}{x'_d}E'_d + \frac{x_q - x'_d}{x'_d}V\sin(¢ - \bar{})\right) \\
\dot{E}_{fd} &= \frac{1}{T_E}\left(V_R - K_E E_{fd}\right)
\end{aligned}
\tag{1}
$$

where ¢ is the error in the rotor angle of the machine, μ is the difference between the generator angular speed and synchronous speed μ_o, P_m and P_e are the mechanical power and active load of the generator, respectively, $M = 2H/\mu_o$ is the generator inertia, E'_q and E'_d are generator's

q- and d-axis flux [4], E_{fd} is the field voltage, and V and $\bar{}$ are the generator bus voltage and phase angle, respectively. The generator electrical power can be calculated [4] as

$$P_{ei} = \frac{1}{x'_d} V \left(E'_q \sin(¢ - \bar{}) - E'_d \cos(¢ - \bar{}) \right) \quad (2)$$

where $B = x'^{-1}_d$ is the generator transient admittance. The bus voltages and phase angles are constrained by the nonlinear algebraic power balance equations.

2.4 Grid-Tie Inverter Model/Observer

The differential equation of the capacitor voltage driven by power balance equation in GTI dc-link (Figure 1) is given by

$$C_{out} v_{out} \frac{dv_{out}}{dt} = P_s - P_e \quad (3)$$

where $P_e = v_{in} VB \sin(¥ - \bar{})$, v_{in} denotes the inverter output voltage, P_s is the solar power injected to the capacitor, ¥ is the inverter ac voltage angle with respect to the grid's slack bus reference, and V and $\bar{}$ represent the voltage and phase angle of the bus connected to the inverter with the reactance B (Figure 1.) The input power P_s is assumed to be provided by a renewable energy source connected to the dc-link. Inverter gain k_{in} and the GTI's ac voltage angle ¥ are two control parameters that can be tuned to control the GTI's voltage and power. That is, the inverter ac voltage magnitude v_{in} (a function of k_{in}) and angle ¥ can be altered to adjust the GTI's power. Voltage conversion relationship in the inverter is given as

$$v_{in} = k_{in} v_{out} \ . \quad (4)$$

The GTI's output power can be controlled in response to the extra power stored in the dc-link capacitor through the control of the GTI's voltage phase angle; i.e.,

$$¥ = ª \tag{5}$$

where auxiliary variable $ª$ is defined to satisfy

$$v_{out}\dot{v}_{out} = \dot{ª} = \frac{1}{C_{out}}(P_s - P_e). \tag{6}$$

In other words, angle $¥$ is defined as a new state variable that acts in a manner similar to angle $¢$ in the SG; that is, it varies with changes in the capacitor's stored energy.

Equations (5) and (6) when compared with dynamics (1) suggest that the GTI resemble a synchronous generator with rotor angle $¥$ and rotor speed $ª$ that can be calculated as

$$ª = (v_{out}{}^2 - v_{outo}{}^2)/2 \tag{7}$$

using (6) with v_{outo} being the steady-state value of the capacitor voltage. In the RG, capacitance C_{out} plays the role of machine inertia M; that is, its higher size reduces the oscillations and contributes to an enhanced dynamic stability. In the SG, the output electric power can be represented in terms of E'_q and E'_d according to (2). In order to attain similarity to the SG, two new auxiliary parameters are defined as E'_{qr} and E'_{dr} allowing the inverter output power to be represented as

$$\overline{P}_e = \frac{1}{x'_{dr}}\left(E'_{qr}\sin(¥ - ¯) - E'_{dr}\cos(¥ - ¯)\right) \tag{8}$$

where parameter x'_{dr} is a RG design parameter. This power needs to represent the GTI output power and be equal to

$$P_e = v_{in}VB\sin(¥ - ¯) \tag{9}$$

i.e., $\overline{P}_e = P_e$. From (8) and (9) the GTI desired ac voltage v_{in} can be written as

$$v_{in} = \frac{E'_{qr}\sin(¥ - ¯) - E'_{dr}\cos(¥ - ¯)}{x'_{dr}\, B\sin(¥ - ¯)} \tag{10}$$

which maintains GTI output power. As only a portion of the total delivered power usually fluctuates in the transients, term $\sin(¥ - ¯)$ does not approach zero and thus no excessive v_{in} is expected from this model.

Finally, according to (4) gain k_{in} can be tuned to adjust the GTI output voltage such that

$$k_{in} = \frac{v_{in}}{v_{out}}. \tag{11}$$

Adjusting gain k_{in} according to (11) allows the GTI to deliver the power governed by (8). According to (1), E'_q and E'_d in SG vary with the excitation voltage E_{fd}. By applying a similar relationship a new state variable for RG can be defined, namely E_{fdr}, as

$$\dot{E}'_{qr} = \frac{1}{T_{d0r}}\left(-\frac{x_{dr}}{x'_{dr}}E'_{qr} + \frac{(x_{dr} - x'_{dr})}{x'_{dr}}V\cos(¥ - ¯) + E_{fdr}\right) \tag{12}$$

which plays a similar role to E_{fd} in SG where parameters x_{dr} and T_{d0r} are RG design parameters and need to be chosen for each RG as opposed to those of SG that are machine parameters and fixed.

In a RG two-axis-like modeling, E'_{dr} can be defined similar to that of the SG which along with equations (5) through (12) forms the dynamics

$$¥ = ª$$

$$ª̇ = \frac{1}{C_{out}}(P_s - P_e) \tag{13}$$

$$\dot{E}'_{qr} = \frac{1}{T_{d0r}}\left(-\frac{x_{dr}}{x'_{dr}}E'_{qr} + \frac{(x_{dr} - x'_{dr})}{x'_{dr}}V\cos(¥ - ¯) + E_{fdr}\right)$$

$$\dot{E}'_{dr} = \frac{1}{T_{q0r}}\left(-\frac{x_{qr}}{x'_{dr}}E'_{dr} + \frac{(x_{qr} - x'_{dr})}{x'_{dr}}V\sin(¥ - ¯)\right)$$

$$\dot{E}_{fdr} = \frac{1}{T_{Er}}\left(V_{Rr} - K_{Er}E_{fdr}\right)$$

where x_{qr} and T_{q0r} are RG design parameters and V_{Rr} is the applied voltage to the RG imaginary excitation system and can be controlled by any of the known SG control methods. Through the synthesized states and input V_{Rr}, an AVR-like mechanism, which takes the GTI's capacitor voltage error as input, can be applied to the RG. As mentioned before, the inverter gain (k_{in}) and ac voltage angle (¥) are the control inputs for the GTI and alter its output voltage and power.

2.5 Renewable Generator Stabilizers

Now the renewable source can be considered as an imaginary synchronous generator and will behave similarly. Next, conventional control strategies for a synchronous generator system can be utilized for this system. Among those methods, AVR+PSS is adopted in this research.

The AVR mechanism is depicted in Figure 2 which can be realized for both SGs and RGs and can incorporate a stabilizing signal from a PSS. For GTI, feedbacks from the output power

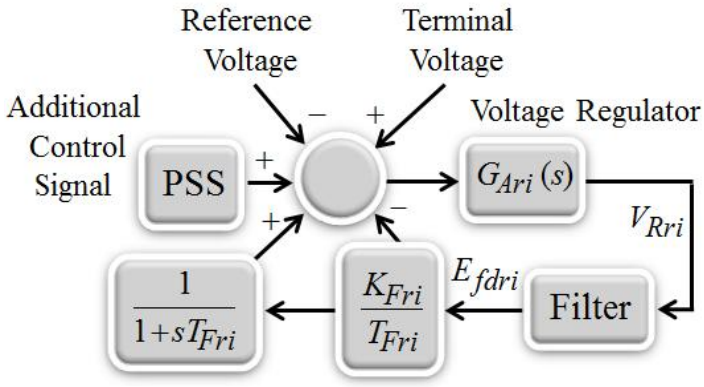

Figure 2 Automatic voltage regulator (AVR) applied to SGs and RGs.

and/or dc-link capacitor voltage provide the PSS with the required stored energy changes and/or delivered power signals.

CHAPTER 3
CONVERTER DISCRETE-TIME CONTROLLER

3.1 Introduction

Usually the maximum power point tracking (MPPT) is desirable for the photovoltaic system steady-state operation. However, without an appropriate controller maximum power point can behave unstably when power oscillations occur in the perturbed power system due to a decrease in generated power when terminal voltage drops as a result of increase in the output power. Yet, regardless of the operating point, the PV terminal voltage can be stabilized and maintained constant by adjusting the duty cycle of the dc-dc converter through a proper stabilizing controller during the moments of power fluctuations caused by disturbances.

3.2 Converter Discrete-Time Model

A typical PV generator with the associated dc-dc buck converter is demonstrated in Figure 3. In order to maintain a constant flow of power to dc-link capacitor C_{out} considering the capacitor voltage fluctuations during disturbances, the duty ratio d of the dc-dc converter needs to be adjusted, dynamically.

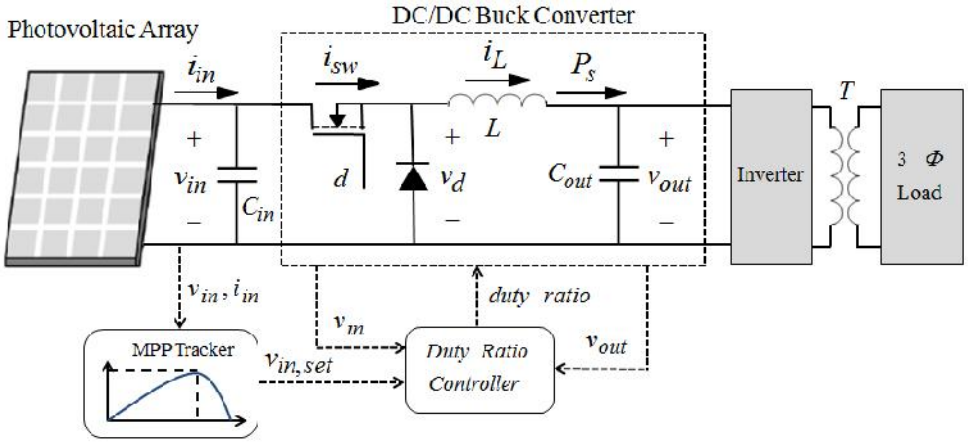

Figure 3 MPPT and dc-dc buck converter control system.

The set point for capacitor C_{in} voltage, namely $v_{in,set}$ is indicated by the MPPT block. Any instantaneous change in the voltage of the GTI dc-link capacitor C_{out} (v_{out}) requires the converter duty ratio *d* adjustment by the controller in such a way that the capacitor C_{in} input power (P_{in}) remains constant. This task can be accomplished by retaining constant voltage at C_{in} (v_{in}) via duty cycle (*d*) controller.

In the rest of this section a nonlinear discrete-time model for the solar-system-connected buck converter is presented assuming a fixed sampling period *T*. Signal *d*, the duty cycle, is a discrete-time control signal and is updated at the beginning of the sampling time. The state variables are the buck converter input capacitor voltage v_{in} and the inductance current i_L (Figure 3) The state variables values $v_{in}(kT)$ and $i_L(kT)$, and the output voltage $v_{out}(kT)$ are sampled at the beginning of the switching period T as shown in Figure 4 where *k* is the sampling index.

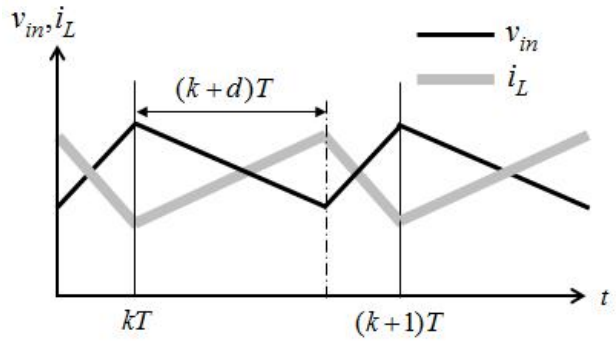

Figure 4 Switching cycle.

The buck converter is assumed to operate in continuous-current mode (CCM.) The photovoltaic array output current $i_{in}(kT)$ (shown in Figure 3) is a function of solar output voltage $v_{in}(kT)$ in the form of [1]

$$i_{in}(kT) = n_p I_s - n_p I_o(e^{v_{in}(kT)/\, n_s V_T} - 1) \tag{14}$$

where n_p and n_s are numbers of the parallel and series arrays forming the PV generator, respectively, V_T is thermal voltage, I_s is the light-generated current and I_o denotes the reverse saturation current [1].

In order to calculate v_{in} at $t = (k+1)T$ the solar current i_{in} can be approximated by its value in the beginning of the switching time ($i_{in}(kT)$) and the switch current i_{sw}, can be estimated by its average value ($d\, i_L(kT)$) during a switching interval. Also, to calculate $i_L((k+1)T)$, the solar diode voltage v_d and the output voltage v_{out} are approximated by $d\, v_{in}(kT)$ and $v_{out}(kT)$, respectively, over the sampling period and are updated at the end of the period T. Therefore, the system can be described by a set of state-space equations

$$v_{in}((k+1)T) = \frac{T}{C_{in}}[i_{in}(kT) - d\, i_L(kT)] + v_{in}(kT) \tag{15}$$

$$i_L((k+1)T) = \frac{T}{L}[d\, v_{in}(kT) - v_{out}(kT)] + i_L(kT) \tag{16}$$

where L and C_{in} are the converter inductance and input capacitor values, respectively, and the photovoltaic array output current $i_{in}(kT)$ is a nonlinear function of $v_{in}(kT)$ as given in (14).

From now on, the switching time T is removed from time index for simplicity; for instance, $v_{in}(kT)$ is shown by $v_{in}(k)$.

3.3 Solar Power Converter Discrete-Time Control Design

The discrete-time model ((15) and (16)) can be controlled by selecting a proper control input *d*. Here voltage v_{in} is controlled whose dynamical equation can be written in the general form

$$x_1((k+1)T) = f(x(kT)) + g(x(kT))u_k \tag{17}$$

where $x(kT) = [x_1(kT)\ \ x_2(kT)]^T = [v_{in}(kT)\ \ i_L(kT)]^T$, $u_k = d$ is the control input, $f(x(kT)) = \frac{T}{C_{in}} i_{in}(kT) + v_{in}(kT)$ and $g(x(kT)) = \frac{-T}{C_{in}} i_L(kT)$ is the control gain. Note that f and g are unknown due to degradation of the converter capacitor C_{in} and variation in the solar panel characteristics. Thus, here an adaptive NN controller is utilized to overcome the unknown dynamics. Define the tracking error as

$$z(kT) = x_1(kT) - x_{1d}(kT). \tag{18}$$

Assumption 1: The input gain $g(x(kT))$ is bounded away from zero and is bounded above in a compact set t. Without loss of generality, we assume that it satisfies

$$0 < g_{\min} \le g(x(kT)) \le g_{\max}. \tag{19}$$

In t where $g_{\min}$ and $g_{\max}$ are positive real constants. Next the controller development is introduced.

In this section, a NN controller that employs the tracking error, NN function approximation capability, and a novel NN weight estimate tuning scheme is developed. The stability criterion is then elaborated to show the stability of the tracking error as well as NN weight estimates.

By using (17) and (18) the tracking error dynamic can be written as

$$z((k+1)T) = g(x(kT))\left(\frac{f(x(kT)) - x_{1d}((k+1)T)}{g(x(kT))} + u \right). \tag{20}$$

The ideal stabilizing control input can be defined as $u = u^* = u_d + K z(kT)$ where $u_d = -g(x(kT))^{-1}\left(f(x(kT)) - x_{1d}((k+1)T) \right)$ with $x_{1d}((k+1)T)$ being the future value of the

desired trajectory $x_{1d}(kT)$. This results in asymptotically stable dynamics in terms of the tracking error $z((k+1)T) = K\,z(kT)$ with $K<1$ being a positive design constant. However, in practical applications u_d is unavailable since the internal dynamics $f(x(kT))$ and control gain matrix $g(x(kT))$ are unknown. Thus, we employ NN function approximation property to approximate u_d as

$$u_d = -g(x(kT))^{-1}\left(f(x(kT)) - x_{1d}((k+1)T)\right) = W^T \circ (x, x_{1d}((k+1)T)) + £ \tag{21}$$

where W is the target NN weight matrix, $\circ(.)$ is the activation function and $£$ is the NN function approximation error. This error can be made small by increasing the number of NN hidden-layer neurons [22] and is ignored in this work for simplicity. In practice, the target weights W is not available and only an estimation of the NN weights is available. Thus, u_d is approximated as $\hat{u}_d$ by using a NN to get u as

$$u = \hat{u}_d + Kz(kT) = \hat{W}^T \circ (x, x_{1d}((k+1)T) + Kz(kT) \tag{22}$$

where $\hat{W}^T$ is the NN weight estimation matrix.

Now define the weight estimation error as $\tilde{W} = \hat{W} - W$. By using (22) tracking error (18) dynamics become

$$z((k+1)T) = f(x(kT)) - x_d((k+1)T) + g(x(kT))\left(\hat{W}^T \circ + Kz + u_d - u_d\right)$$

$$= g(x(kT))\left(\tilde{W}^T \circ + Kz\right). \tag{23}$$

Next define the NN weight update law as

$$\hat{W}((k+1)T) = c\hat{W}(kT) - c^{-1}\sim \circ\ z((k+1)T) \tag{24}$$

where $c<1$ is a positive design constant. By subtracting the target weights from (24), we have

$$\tilde{W}((k+1)T) = c\tilde{W}(kT) - c^{-1}\tilde{\circ}\ z((k+1)T) - (1-c)W\ . \tag{25}$$

The presence of the parameter $c < 1$ in the above update law (24) prevents the NN weight estimates from remaining large after the regulation error becomes small, as opposed to conventional update laws [16],[5] where $c = 1$.

3.4 Stability Analysis

In this part we present the stability of the nonlinear discrete-time system (17) and the NN weights where the tracking error $z(kT)$ and weight estimation error $\tilde{W}(kT)$ are bounded in the presence of unknown internal dynamics $f(x(kT))$ and control gain matrix $g(x(kT))$.

Definition. **(Uniform Ultimate Bounded (UUB)**). Consider the dynamical system $x(k+1) = f(x)$ with $x \in \Re^n$ being a state vector. Let the initial time step be k_0 and initial condition be $x_0 = x(k_0)$. Then, the equilibrium point x_e is said to be UUB if there exists a compact set $S \subset \Re^n$ so that for all $x_0 \in S$ there exists a bound B and a time step $K(B, x_0)$ such that $\|x(k) - x_e\| \le B$ for $\forall k > k_0 + K$.

Definition. (**Lyapunov Stability**) Consider a function $L(x) : R^n \to R$ such that $L(0) = 0$, $L(x) \ge 0$ (positive definite) and $\dot{L}(x) = \frac{d}{dt}L(x) \le 0$ (negative definite) ; equality happens if and only if $x = 0$. Then $L(x)$ is called a Lyapunov function candidate and the system is asymptotically stable in the sense of Lyapunov.

The following theorem guaranties boundedness of the weight estimation errors $\tilde{W}(kT)$ and the tracking errors $z(kT)$. Next the following theorem can be stated.

Theorem 1 (NN State Feedback Controller Stability): Consider the nonlinear discrete-time system given by (17). Let the Assumptions 1 hold and the desired trajectory x_{1d} and initial conditions for system (17) be bounded in the compact set t. Let the unknown nonlinearities be approximated by a NN whose weight update is provided by (24). Then there exist a control gain K associated with the given control inputs (22) such that the tracking error $z(kT)$ as well as the NN weight estimation error $\tilde{W}$ are UUB.

Proof. Define the overall Lyapunov function candidate $L = L_W + L_r$, where $L_r(k) = \dfrac{z^2(k)}{g(x(k-1))}$ and $L_W(k) = \dfrac{1}{\sim}\tilde{W}^T(k)\tilde{W}(k)$. Then, the first difference of the Lyapunov function due to the first term becomes

$$\mathsf{a}L_r = \frac{z^2(k+1)}{g(x(k))} - \frac{z^2(k)}{g(x(k-1))}. \tag{26}$$

Substituting the tracking error (23) into (26) and expanding the terms, we obtain

$$\mathsf{a}L_r = g(k)(\tilde{W}^T \circ (x) + Kz)^2 - \frac{z^2(k)}{g(k-1)}. \tag{27}$$

Next, by using (15), the first difference due to the second term in the overall Lyapunov function candidate is obtained as

$$\mathsf{a}L_W = \frac{1}{\sim}\left\| c\ \tilde{W}(k) - c^{-1}\sim \circ\ z(k+1) - (1-c)W \right\|^2 - \frac{1}{\sim}\tilde{W}^T(k)\tilde{W}(k). \tag{28}$$

Expanding the first difference of the overall Lyapunov function candidate $\mathsf{a}L = \mathsf{a}L_r + \mathsf{a}L_W$ by using (26) and (27) to get

$$\mathsf{a}L_W = \frac{1}{\sim}\left\| c\ \tilde{W}(k) - c^{-1}\sim \circ\ z(k+1) - (1-c)W \right\|^2 - \frac{1}{\sim}\tilde{W}^T(k)\tilde{W}(k)$$

$$\Delta L \le g(k)\circ^{T}\tilde{W}\ \tilde{W}^{T}\circ + g(k)K^{2}z^{2} + 2g(k)\tilde{W}^{T}\circ Kz - \frac{z^{2}(k)}{g(k-1)}$$

$$+\frac{c^{2}}{\sim}\tilde{W}^{T}(k)\tilde{W}(k) + \sim c^{-2}\circ^{T}\circ\left[g(x(k))\left(\tilde{W}^{T}\circ(x)+Kz\right)\right]^{2}$$

$$+\frac{1}{\sim}(1-c)^{2}\|W\|^{2} - 2\tilde{W}^{T}(k)\circ\left[g(x(k))\left(\tilde{W}^{T}\circ(x)+Kz\right)\right] \qquad (29)$$

$$+2\|\tilde{W}\|\frac{\|c(1-c)\|}{\sim}\|W\| + 2W^{T}(1-c)c^{-1}\circ\left[g(x(k))\left(\tilde{W}^{T}\circ(x)+Kz\right)\right] - \frac{1}{\sim}\tilde{W}^{T}(k)\tilde{W}(k).$$

Applying the Cauchy-Schwarz inequality $(a_1 + a_2 + \cdots + a_n)^2 \le n(a_1^2 + a_2^2 + \cdots + a_n^2)$ and

$\circ^{T}\tilde{W}\tilde{W}^{T}\circ = \tilde{W}^{T}\circ\circ^{T}\tilde{W}$, yields

$$\Delta L \le \frac{1}{\sim}(1-c)^{2}\|W\|^{2} + \frac{c(1-c)}{\sim}\|W\|^{2} + (1-c)c^{-1}\|W\|^{2}\|\circ\|^{2}$$

$$+\begin{pmatrix}2+g(k)+g_i(k)^2+4(1-c_i)c_i^{-1}g_i(k)^2\\ +4\sim c^{-2}\|\circ\|^{2}g(k)^2\end{pmatrix}K^{2}z^{2} - \frac{z^{2}(k)}{g(k-1)} - \frac{1-c}{\sim}\tilde{W}^{T}(k)\tilde{W}(k)$$

$$-\left(g(k) - 4(1-c)c^{-1}g(k)^2 - 4\sim c^{-2}\|\circ\|^{2}g(k)^2\right)\tilde{W}^{T}(k)\circ\circ^{T}\tilde{W}(k). \qquad (30)$$

Thus, (30) becomes

$$\Delta L \le \frac{1}{\sim}(1-c)^{2}\|W\|^{2} + \frac{c(1-c)}{\sim}\|W\|^{2} + (1-c)c^{-1}\|W\|^{2}\|\circ\|^{2}$$

$$+\begin{pmatrix}2+g(k)+g_i(k)^2+4(1-c_i)c_i^{-1}g_i(k)^2\\ +4\sim c^{-2}\|\circ\|^{2}g(k)^2\end{pmatrix}K^{2}z^{2} - \frac{z^{2}(k)}{g(k-1)} - \frac{1-c}{\sim}\|\tilde{W}(k)\|^{2}$$

$$-\left(g(k) - 4(1-c)c^{-1}g(k)^2 - 4\sim c^{-2}\|\circ\|^{2}g(k)^2\right)\|\circ\|_{\max}^{2}\|\tilde{W}(k)\|^{2}$$

$$\le -(C_z' z^{2} + C_w'\|\tilde{W}(k)\|^{2} - C_{\pounds}') \qquad (31)$$

where

$$C'_{\mathcal{E}} = \frac{1}{\sim}(1-c)^2 \| W \|^2 + \frac{c\ (1-c)}{\sim} \| W \|^2 + (1-c)c^{-1} \| W \|^2 \| \circ \|^2_{\max} \ ,$$

$$C'_z = \frac{1}{g_{\max}} - \left(1 + g_{\max} + g_{\max}{}^2 + 4(1-c)c^{-1} g_{\max}{}^2 + 4\sim\ c^{-2} \| \circ \|^2_{\max} g_{\max}{}^2 \right) K_i{}^2 ,$$

$$C'_w = \frac{1-c}{\sim} + C'_{\circ w} ,$$

and

$$C'_{\circ w} = \left(g_{\min} - 4(1-c)c^{-1} g_{\max}{}^2 - 4\sim\ c^{-2} \| \circ \|^2_{\max} g_{\max}{}^2 \right) \| \circ \|^2_{\max} .$$

Therefore, $\dot{V} L \le 0$ in (16) provided the following conditions

$$|z| > \sqrt{\frac{C'_{\mathcal{E}}}{C'_z}} \qquad \text{or} \qquad \left\| \tilde{W}^T(k) \right\| > \sqrt{\frac{C'_{\mathcal{E}}}{C'_w}} . \tag{32}$$

This guaranties the boundedness of the weight estimation errors, $\tilde{W}(kT)$, and shows that the tracking errors $z(kT)$ are UUB.

Hence the Lyapunov stability analysis shows that the proposed NN controller guarantees that the closed-loop signals are UUB with the bounds given by (32). In order to guarantee the UUB results with small bound, the bound $C'_{\mathcal{E}}$ must be reduced. This can be achieved if the constant c is selected to be close to one, whereas K and $\sim$ are selected to be small positive constants which, in turn, causes the stability bounds (32) to decrease.

CHAPTER 4
SIMULATION RESULTS

4.1 Introduction

In order to confirm the theoretical analysis and control design, the solar power generation system is tested in the Matlab Simulink environment. The solar system shown in Figure 1 is connected to a three phase load.

4.2 System Parameters

The model introduced in chapter 2 is now utilized to design damping controller for the inverter. An AVR+PSS mechanism is used to control the terminal voltage using the feedback from the inverter terminal voltage. This mechanism is depicted in Figure 2 which resembles the AVR in the synchronous generators.

As discussed in chapter 2, E_{fdr} controls the inverter gain k_{in} which is comparable to the effect of excitation E_{fd} on E'_q in the generators. Block $G_{Ar}(s)$ is a PI controller and the Filter block in Figure 2 providing E_{fdr} has the following function that was mentioned in (13)

$$\dot{E}_{fdr} = \frac{1}{T_{Er}}\left(V_{Rr} - K_{Er}E_{fdr}\right). \tag{33}$$

In addition, other controllers can be incorporated through feedbacks from the output power or capacitor dc voltage through the “Additional Control Signal” block. Here, the additional control signal is a PSS-like mechanism that receives feedback from the mentioned variables.

The inverter gain (k_{in}) and the angle of inverter voltage (¥) are tuned to satisfy equations (4) and (5) and a PSS is utilized in the renewable generator controller. According to (13), the size of the capacitor plays the role of moment of inertia (M), and thus, it acts as energy

storage. The renewable generator data are given as $x'_{dr} = 0.06$, $x_{dr} = 0.2$, $x_{qr} = 0.19$, $T_{d0r} = 7$, $K_{Er} = 1$, $T_{Er} = 0.75$ and $H = \mu_s M/2 = 5$ p.u. The AVR is defined by $G_{\mathrm{Ar}}(s) = 80/(1 + .01s)$, $K_{Fr} = 0.03$ and $T_{Fr} = 10$ .The speed signal input to the PSS is provided by the state a from the observer. Also, $L = 600$ «H, $C_{in} = C_{out} = 1000$ «F the operational frequency of the converter is set to $T = 10$ *kHz* and the load is a three-phase resistive load with $R = 6\ \Omega$ on each phase in steady state condition. The solar module is designed to generate its maximum power $P_{s,mpp} = 1146$ *W* when its voltage is set to $v_{in,mpp} = 121$ *V* .

The control objective is to damp the converter capacitor voltage error caused by the disturbance besides maintaining the solar power constant after a disturbance or load change. In order to evaluate the effectiveness of the controller, the three phase load changes from $R = 6\ \Omega$ to $R = 5.3\ \Omega$ on each phase at $t = 1.4s$. In Figures 5 to 14 the efficiency of the proposed converter modeling and control is compared with the case in which the converter works with a constant duty cycle without any control. The PV array can operate under lower or higher voltage than the MPP voltage. In the results of Figures 5 through 9 the solar voltage is slightly less than the MPP voltage, and for Figures 10 through 14 the solar array operates at a higher voltage than the MPP voltage. In both cases the solar source provides a constant power to the GTI during the transients by using the proposed dc-dc converter controller.

4.3 Solar Voltage Less than MPP Voltage

In this case the solar operating voltage is $v_{in,set} = 116\,V$. After the load change, the controller adjusts the converter duty cycle during a transient interval, in order to maintain the converter input voltage at its set point $v_{in,set} = 116$ *V* (Figure 6) resulting in constant converter

power (Figure 5); whereas, in the constant duty cycle scenario these values do not remain constant after the load change and the PV generator will operate at a different operating point.

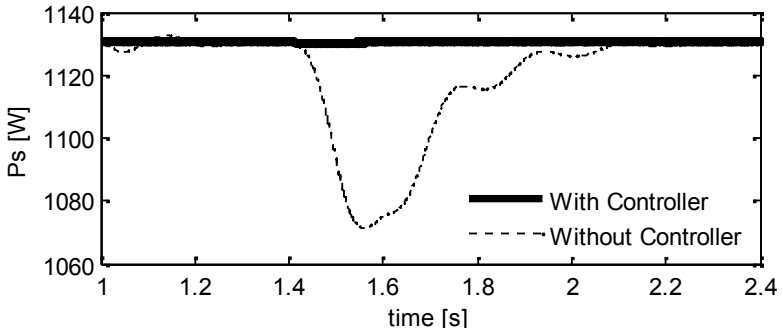

Figure 5 Converter input power, dashed: without controller, solid: with controller; solar voltage is less than MPP voltage.

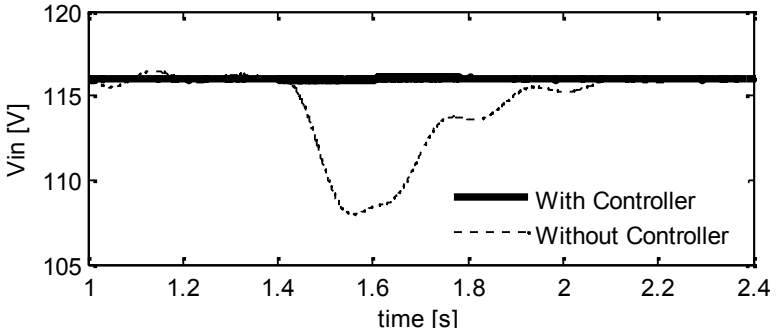

Figure 6 Converter input voltage v_{in}, dashed: without controller, solid: with controller; solar voltage is less than MPP voltage.

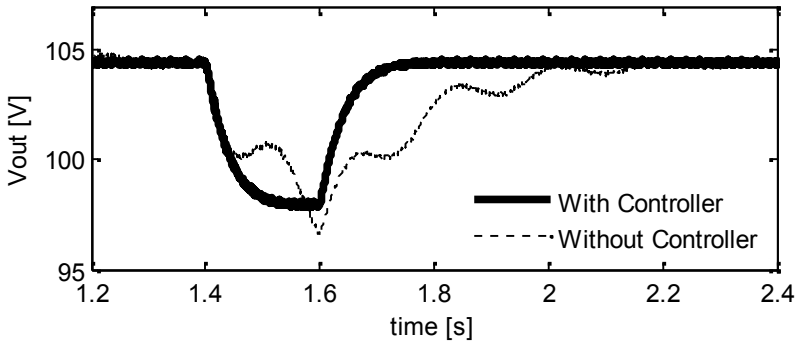

Figure 7 Converter output voltage v_{out}, dashed: without controller, solid: with controller; solar voltage is less than MPP voltage.

Furthermore, the converter output voltage v_{out} changes with faster transients as shown in Figure 7. The converter inductor current i_L and solar input current i_{in} are depicted in Figures 8

and 9, respectively. The fast and accurate operation of the controller shows its effectiveness and implies that the converter power and input voltage are well retained at their desired set points.

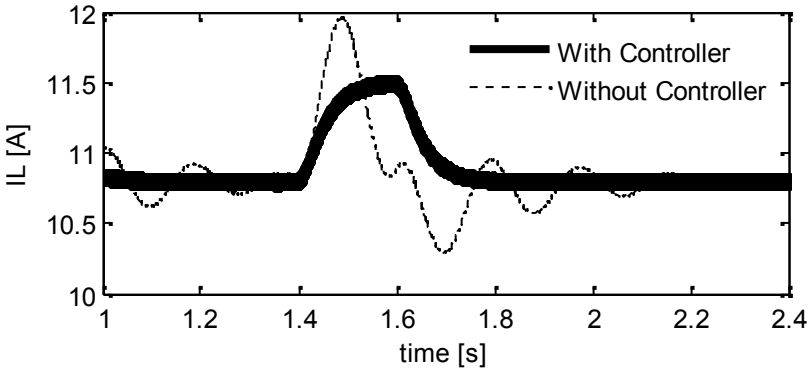

Figure 8 Converter inductor current i_L, dashed: without controller, solid: with controller; Solar voltage is higher than MPP voltage.

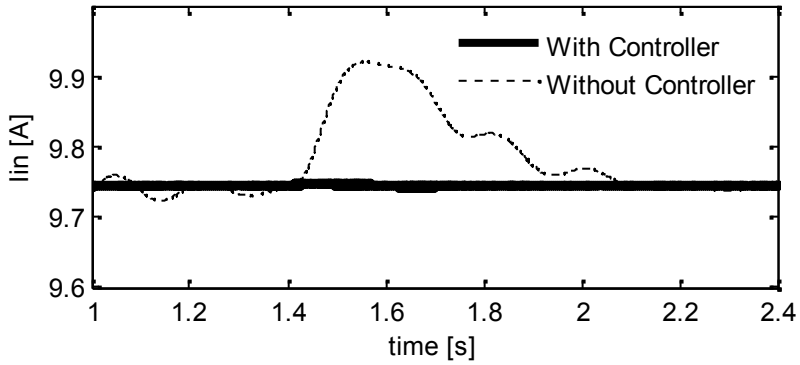

Figure 9 Solar output current i_{in}, dashed: without controller, solid: with controller; solar voltage is higher than MPP voltage.

4.4 Solar Voltage Higher than MPP Voltage

In the second test the solar operating voltage is $v_{in,set} = 131\ V$. As Figure 10 shows, in constant duty cycle condition, the load change causes power change, while the controller adjusts the duty cycle value to the new load condition to maintain the converter power and voltage constant.

The results imply that the controller mitigates oscillations caused by load change faster and presents a significantly better transient response than the system without controller.

Moreover, the proposed controller does not require any data about the new load condition and adjusts the duty cycle according to the desired input voltage and power; whereas, for the system without controller the duty cycle value must be estimated accurately based on load awareness.

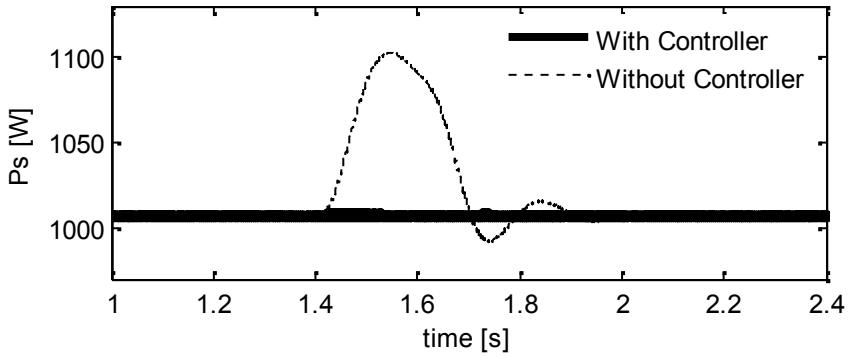

Figure 10 Converter input power, dashed: without controller, solid: with controller; solar voltage is higher than MPP voltage.

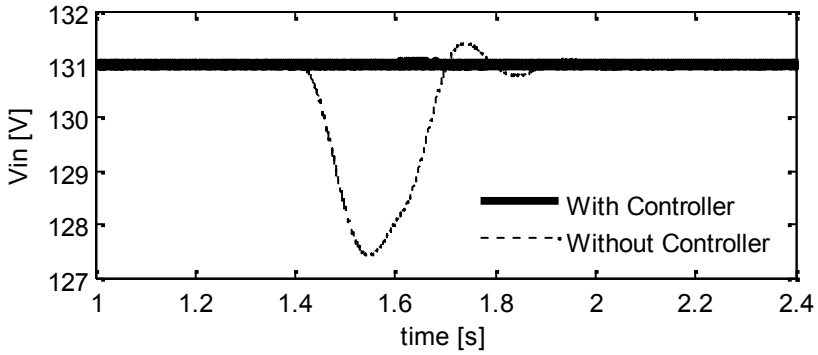

Figure 11 Converter input voltage v_{in}, dashed: without controller, solid: with controller; solar voltage is higher than MPP voltage.

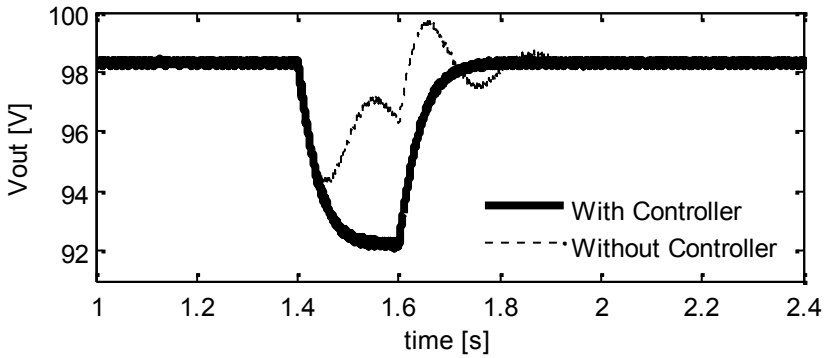

Figure 12 Converter output voltage v_{out} dashed: without controller, solid: with controller; solar voltage is higher than MPP voltage.

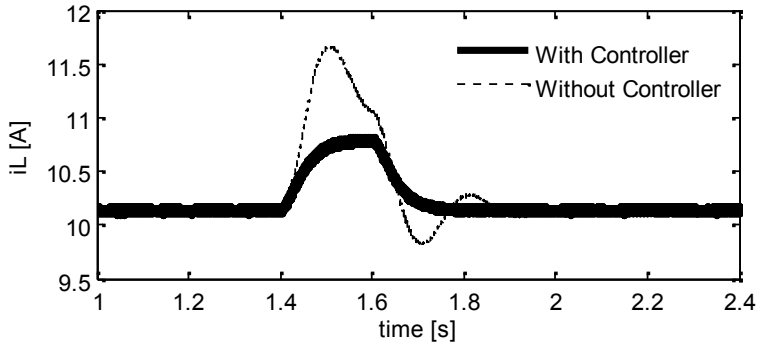

Figure 13 Converter inductor current i_L, dashed: without controller, solid: with controller; solar voltage is higher than MPP voltage.

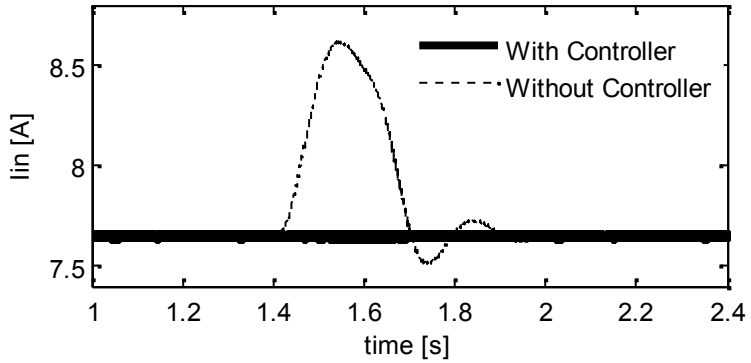

Figure 14 Solar output current i_{in}, dashed: without controller, solid: with controller; solar voltage is higher than MPP voltage.

4.5 Input Voltage Adjustment to Load Change

When the load experiences a change the controller is expected to adjust the to the new load level to maintain the constant input voltage for the converter. In order to show the ability of the controller to automatically adjust to different operating points, the load level has been altered. Load set to $R=5.3\,\Omega$ on each branch changes to $R=4.6\,\Omega$ at t=1.4s, increases to $R=6\,\Omega$ at t=1.8, and goes back to $R=5.3\,\Omega$ at t=2.2s. The results are depicted in Figures 15 to 19 compare the proposed controller performance with the case in which the duty cycle is constant for each value of load. The new duty cycle value for each amount of load must be adjusted to maintain the converter power constant. The results imply that the controller mitigates oscillations caused by load change faster and presents a significantly better transient response than the system

without controller. Moreover, the proposed controller does not require any data about the new load condition and adjusts the duty cycle according to the desired input voltage and power; whereas, for the system without controller the new duty cycle value must be estimated accurately based on new load awareness.

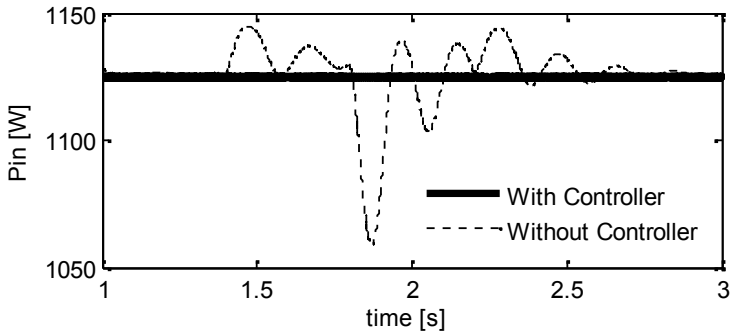

Figure 15 Converter input power adjustment to load change, dashed: without controller, solid: with controller; solar voltage is higher than MPP voltage.

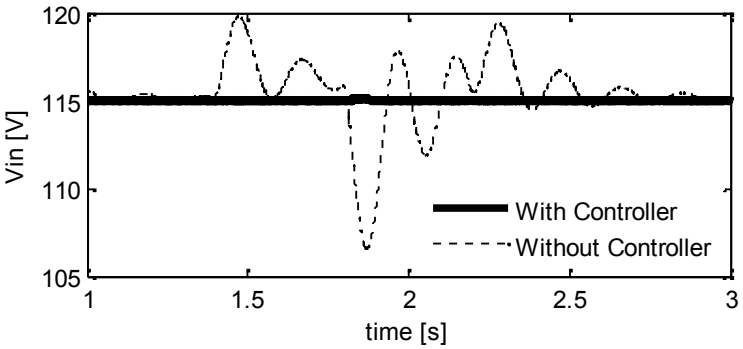

Figure 16 Converter input voltage v_{in} adjustment to load change, dashed: without controller, solid: with controller; solar voltage is higher than MPP voltage.

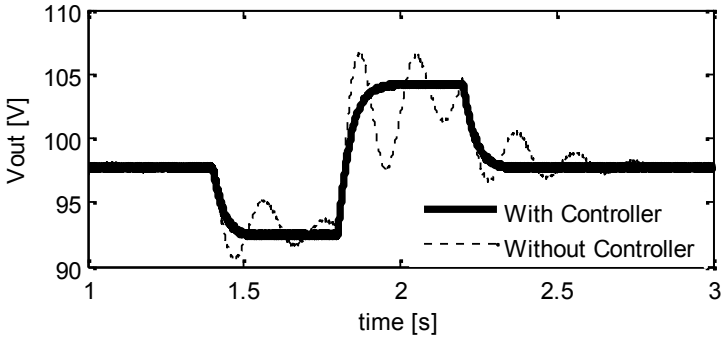

Figure 17 Converter output voltage v_{out} adjustment to load change dashed: without controller, solid: with controller; solar voltage is higher than MPP voltage.

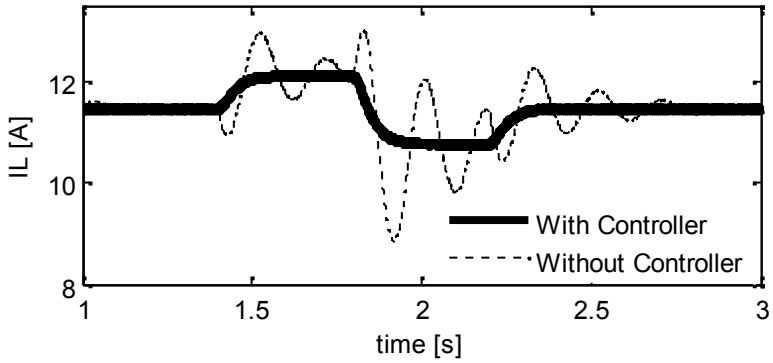

Figure 18 Converter inductor current i_L adjustment to load change, dashed: without controller, solid: with controller; solar voltage is higher than MPP voltage.

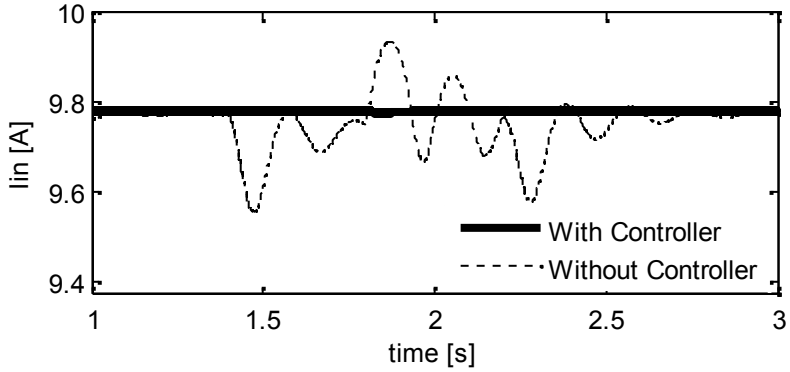

Figure 19 Solar output current i_{in} adjustment to load change, dashed: without controller, solid: with controller; solar voltage is higher than MPP voltage.

Overall, the simulation results show a good control performance provided by the proposed adaptive NN controller and stability of the interconnected dc grid is verified.

CHAPTER 5
CONCLUSIONS AND FUTURE WORK

5.1 Conclusions

In this research the power system contained synchronous and renewable generators is investigated. a GTI is used to interface the renewable energy source to the grid in order to control the delivered power. In order to adjust the operating point of the PV generator, a dc-dc converter is incorporated to the system as an interface between the solar array and the GTI connecting the solar array to the power network. A nonlinear discrete-time model of a photovoltaic-connected buck converter and its stabilizing controller design is presented. The interaction of the solar array dc-dc converter with the GTI is addressed. Simulation results show improved performance and stability of the proposed converter discrete-time controller over the conventional methods in the presence of the power system disturbance. The theoretical conjectures and simulation results of the controller imply that the converter input voltage and power as well as the inductor current are stabilized desirably at their initial set points, which verifies the accuracy of the converter discrete-time model and the effectiveness of the proposed discrete-time controller.

5.2 Recommendation of Future Work

The following recommendations are made for possible future research:

- Discrete-time adaptive neural network is a relatively new topic in the power system stability and control and hence further research can be made to improve its efficiency and effectiveness.
- The system model can be developed to a more general distributed generation system where other renewable or synchronous generators all are interconnected. In this case each system is influenced by other subsystem’s states and a more general control method is necessary.

- The solar system connected dc-dc converter can be modeled in a dc distribution system with interconnected subsystems working in high penetration of renewable generation.

REFERENCES

[1] H. De Battista and R. J. Mantz, "Variable structure control of a photovoltaic energy converter," IEE Proceedings-Control Theory and Applications, vol. 149, pp. 303-310, July 2002.

[2] M. Veerachary, "Power tracking for nonlinear PV sources with coupled inductor SEPIC converter," IEEE Transactions on Aerospace and Electronic Systems, vol. 41, pp. 1019-1029, July 2005.

[3] S. Acevedo and M. Molinas, "Power electronics modeling fidelity: Impact on stability estimate of micro-grid systems," In Innovative Smart Grid Technologies Asia (ISGT), 2011 IEEE PES, 2011, pp.1-8.

[4] S. Kazemlou and S. Mehraeen, “Stability of multi-generator power system with penetration of renewable energy sources, ” Proc. of Power and Energy Society General Meeting, 2012 IEEE, pp.: 1-6, 2012.

[5] S. Jagannathan “Decentralized Discrete-Time Neural Network Controller for a Class of Nonlinear Systems with Unknown Interconnections", Proceedings of the 2005 IEEE International Symposium on Intelligent Control, pp.268 – 273, 2005.

[6] S. Jagannathan, Neural Network Control of Nonlinear Discrete-time Systems, CRC Press, April 2006.

[7] W. M. Lin, C. M. Hong, and C. H. Chen, "Neural-network-based mppt control of a stand-alone hybrid power generation system," IEEE Transactions on Power Elec., vol. 26, pp. 3571-3581, December 2011.

[8] P. K. Peter and V. Agarwal, "On the input resistance of a reconfigurable switched capacitor dc-dc converter-based maximum power point tracker of a photovoltaic source," IEEE Transactions on Power Electronics, vol. 27, pp. 4880-4893, December 2012.

[9] C. C. Hua, J. G. Lin, and C. M. Shen, "Implementation of a DSP-controlled photovoltaic system with peak power tracking," IEEE Transactions on Industrial Electronics, vol. 45, pp. 99-107, Feburary 1998.

[10] M. Karppanen, J. Arminen, T. Suntio, K. Savela, and J. Simola, "Dynamical modeling and characterization of peak-current-controlled superbuck converter," IEEE Transactions on Power Electronics, vol. 23, pp. 1370-1380, May 2008.

[11] E. Koutroulis, K. Kalaitzakis, and N. C. Voulgaris, "Development of a microcontroller-based, photovoltaic maximum power point tracking control system," IEEE Transactions on Power Electronics, vol. 16, pp. 46-54, January 2001.

[12] Z. J. Qian, O. Abdel-Rahman, H. Al-Atrash, and I. Batarseh, "Modeling and Control of Three-Port DC/DC Converter Interface for Satellite Applications," IEEE Transactions on Power Electronics, vol. 25, pp. 637-649, March 2010.

[13] M. Veerachary, T. Senjyu, and K. Uezato, "Neural-network-based maximum-power-point tracking of coupled-inductor interleaved-boost-converter-supplied PV system using fuzzy controller," IEEE Transactions on Industrial Electronics, vol. 50, pp. 749-758, August 2003.

[14] C. S. Chiu, "T-S fuzzy maximum power point tracking control of solar power generation systems," IEEE Transactions on Energy Conversion, vol. 25, pp. 1123-1132, December 2010.

[15] S. V. Iyer, M. N. Belur and M. C. Chandorkar, "A generalized computational method to determine stability of a multi-inverter microgrid," IEEE Transactions on Power Elec., vol. 25, no. 9, September 2010.

[16] E. Barklund, N. Pogaku, M. Prodanovic´, C. Hernandez-Aramburo and T. C. Green, "Energy management in autonomous microgrid using stability-constrained droop control of inverters," IEEE Transactions on Power Electronics, vol. 23, no. 5, September 2008.

[17] I-Y. Chung, W. Liu and D. Cartes, " Control methods of inverter-interfaced distributed generators in a microgrid system," IEEE Transactions on Industry Application, vol.45, no.:3, May/June, 2010.

[18] E. Serban and H. Serban,, " A control strategy for a distributed power generation microgrid application with voltage and current-controlled source converter, " IEEE Transactions on Power Electronics , vol.25, no.12, December 2010.

[19] K. Kurohane , T. Senjyu, A. Yona, N. Urasaki, T. Goya, and T. Funabashi, "A hybrid smart ac/dc power system," IEEE Transactions on Smart Grid, vol. 1, no. 2., pp.: 199-2014, 2010.

[20] F. Chierchie and E. E. Paolini, "Discrete-time modeling and control of a synchronous buck converter," Proceedings of the Argentine School of Micro-Nanoelectronics, Technology and Applications, pp: 5-10, 2009.

[21] M. Veerachary, "Two-Loop Controlled Buck–SEPIC Converter for Input Source Power Management," IEEE Transactions on Industrial Electronics, vol. 59, no. 11, November 2012.

[22] F. Lewis, S. Jagannathan, S., and A. Yesildirek, "Neural Network Control of Robot. Manipulators and Nonlinear Systems", Taylor & Francis, 1998.

THE VITA

Shaghayegh Kazemlou was born in 1984 in Iran. She received her BSc and MSc degree from Sharif University of Technology in Engineering Engineering, in 2007 and 2010, respectively. She is currently a PhD candidate in Louisiana State University at the Electrical and Computer Engineering Devision.